

Analysis of Transfer Reactions: Determination of Spectroscopic Factors

N. Keeley

CEA Centre de Saclay, DSM/DAPNIA/SPhN, F-91191 Gif-sur-Yvette, France

and

Department of Nuclear Reactions, The Andrzej Sołtan Institute for Nuclear Studies, ul. Hoża 69, 00-681 Warsaw, Poland

Abstract. An overview of the more popular models used for the analysis of direct reaction data is given, concentrating on practical aspects. As a concrete example, the $^{12}\text{C}(\text{d,p})^{13}\text{C}$ reaction at an incident deuteron energy of 30 MeV is analysed with progressively more physically sophisticated models. The effect of the choice of reaction model on the spectroscopic information extracted from the data is investigated and other sources of uncertainty in the derived spectroscopic factors are discussed.

Résumé. En nous focalisant sur les aspects pratiques, nous effectuons une revue des modèles les plus couramment utilisés pour l'analyse des données de réactions directes. Nous utilisons comme illustration la réaction $^{12}\text{C}(\text{d,p})^{13}\text{C}$, avec un deuton incident de 30 MeV, en l'analysant avec des modèles physiquement de plus en plus complexes. Les conséquences du modèle de réaction choisi sur l'information spectroscopique extraite des données sont mises en évidence. Les autres sources d'incertitude sur les facteurs spectroscopiques extraits sont également discutées.

SCOPE OF THE LECTURES

These lectures are intended to give a brief overview of some of the more commonly used direct reaction models, concentrating on their use in practice to extract spectroscopic factors from angular distribution data. They will not present details of the formalism underlying these models which are given in a number of text books; two that I have found particularly useful are those by Hodgson [1] and Satchler [2]. A number of practical examples will be presented where the same data are analysed by progressively more sophisticated reaction models and the sources of uncertainty in the derived spectroscopic quantities are discussed. The ultimate aim of these lectures is to present the reader with sufficient information to enable analyses of direct reaction data in the literature to be assessed critically — in the best sense of the term — according to the following criteria:

1. Is the reaction model used appropriate to the circumstances?
2. What are the likely uncertainties in the derived spectroscopic quantities?
3. Are the conclusions drawn fully justified by the analysis?

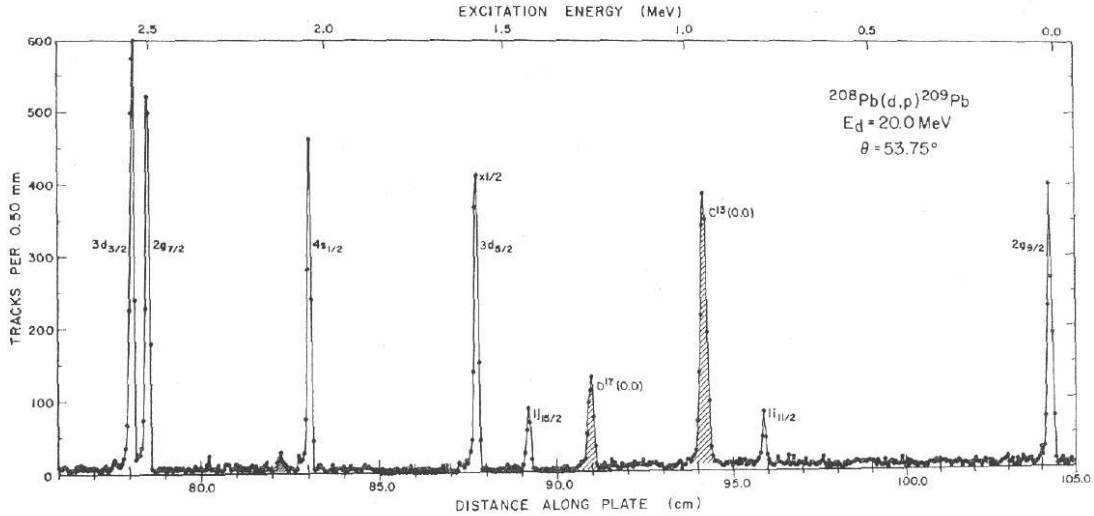


FIGURE 1. Proton spectrum for the $^{208}\text{Pb}(d,p)^{209}\text{Pb}$ reaction at an incident deuteron energy of 20 MeV. The two shaded peaks represent reactions from Carbon and Oxygen contaminants in the target. Taken from Ref. [3].

INTRODUCTION: DIRECT REACTIONS AS A SPECTROSCOPIC TOOL

Direct reactions are particularly useful as a spectroscopic tool due to their selectivity – they favour the population of single particle (or hole) levels, see Fig. 1. Spectroscopic information concerning the single-particle nature of the observed levels may then be compared with the results of structure model calculations. Such measurements are particularly useful if it is possible to locate and identify all the states in a given nucleus that have appreciable single particle strength. If this can be done one may, for example, determine the extent to which each shell model orbital is filled in the target nucleus. Apart from the excitation energies of the states, directly obtainable from energy-calibrated spectra, how does one obtain the desired information — spin, parity, spectroscopic factor — from the direct reaction data?

It was first demonstrated by Butler [4] that the measured angular distributions of the differential cross section ($d\sigma/d\Omega$) of the $^AZ(d,p)^{A+1}Z$ transfer reaction depend sensitively on L , the angular momentum of the transferred neutron with respect to the “core” nucleus AZ , thus enabling L to be determined by a comparison of the measured angular distribution with one calculated by a suitable model of the reaction, see Fig. 2. This L dependence is not restricted to the (d,p) process and is a general feature of transfer reactions. If we know L we may determine the parity of the residual state via the relation:

$$\pi_T \pi_R = (-1)^L \quad (1)$$

where π_T and π_R are the parities of the target and residual states. However, the total spin of the residual state, J_R , is not in general unambiguously determined, being given by the

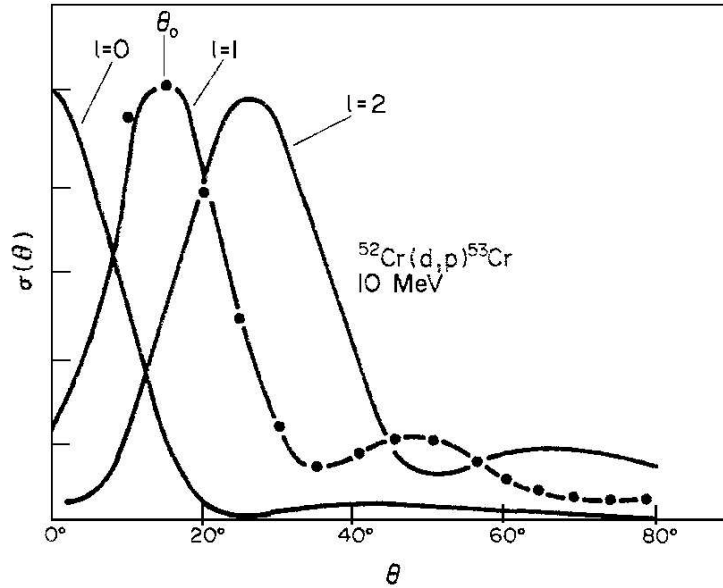


FIGURE 2. Cross section measurement (points) and DWBA calculations (curves) for $^{52}\text{Cr}(d,p)^{53}\text{Cr}$ illustrating the dependence of the peak position on L . Taken from Ref. [5].

vectorial relation:

$$\mathbf{J}_R = \mathbf{J}_T + \mathbf{L} + \mathbf{s} \quad (2)$$

where \mathbf{J}_T is the total spin of the target state and \mathbf{s} is the intrinsic spin of the transferred particle. In the case of a (d,p) reaction on an even-even target where $s = 1/2$ and $J_T = 0$ this reduces to:

$$J_R = L \pm 1/2. \quad (3)$$

The general case is considerably more complicated, and a state of given J_R may have contributions from two or more different L values or, conversely, a given L may couple with a non-zero J_T to give several states with different J_R values. Thus a measurement of the differential cross section alone is not usually sufficient to determine J_R completely.

Although a systematic J -dependence of the cross section angular distribution at large angles has been noted for $L = 1$ (d,p) reactions [6] the principal means of determining J_R is by measurement of the vector analysing power iT_{11} [7] in an experiment with a polarised deuteron beam or target. The vector analysing power may be defined as:

$$iT_{11} = \frac{1}{2\sqrt{3}} \frac{\sigma_{\text{UP}} - \sigma_{\text{DOWN}}}{\sigma_0} \quad (4)$$

where σ_{UP} and σ_{DOWN} refer to the cross section measured with a deuteron beam that is fully polarised parallel (UP) or antiparallel (DOWN) to \hat{y} , where the y -axis is chosen to be perpendicular to the reaction plane (see Fig. 3). The quantity σ_0 denotes the cross section for an unpolarised beam.

Figure 4 shows some typical results for $L = 1$ transitions in the $^{52}\text{Cr}(d,p)^{53}\text{Cr}$ reaction. Note that while the form of the cross section angular distributions is essentially identical for all three transitions that of the analysing power is characteristic of the J_R value;

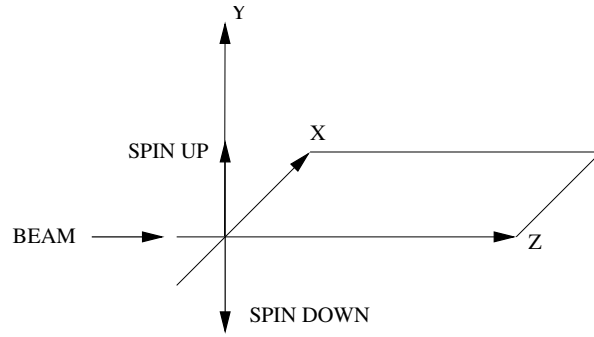


FIGURE 3. Coordinate system for the calculation of iT_{11} , adapted from [5].

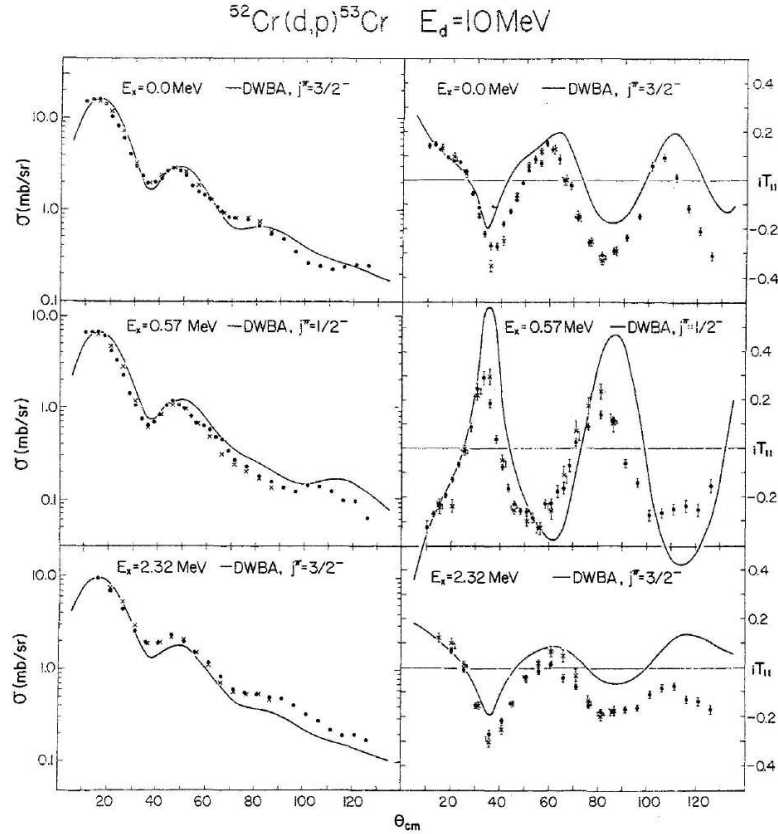


FIGURE 4. Cross section and vector analysing power measurements for three $L = 1$ $^{52}\text{Cr}(d,p)^{53}\text{Cr}$ transitions illustrating the dependence of analysing power on J_R . Taken from Ref. [5].

the two $J_R = 3/2$ transitions have similar vector analysing powers whereas iT_{11} for the $J_R = 1/2$ transition has the opposite sign.

Such measurements require either a polarised deuteron beam (in conventional kinematics for stable target nuclei) or a polarised deuteron target for radioactive beam experiments carried out in inverse kinematics. While polarised deuteron targets are under serious consideration for a number of current and proposed radioactive beam facilities

their practical application is still several years in the future, therefore we shall not consider this aspect in detail. Knutson and Haeberli [5] give a useful review of polarisation effects in transfer reactions for those who wish to pursue this subject.

The final quantity that we wish to determine is the spectroscopic factor, S_{JL} . It is a direct measure of the single-particle purity of the final, i.e. residual (or initial, i.e. target) state. In its most basic form S_{JL} is defined by the following relation:

$$d\sigma(\theta, E)/d\Omega = S_{JL}F_{JL}(\theta, E) \quad (5)$$

where $d\sigma(\theta, E)/d\Omega$ is the differential cross section and $F_{JL}(\theta, E)$ is a factor that depends on the reaction mechanism and contains all the angular and energy dependence. A measurement of the transfer cross section combined with the calculation of $F_{JL}(\theta, E)$ by a suitable reaction model enables the spectroscopic factor to be determined, provided that the quantum numbers J and L are known. Depending on the precise definition, S_{JL} often includes the isospin Clebsch-Gordan coefficient, C , and is therefore sometimes written as C^2S . Also, in practice S_{JL} is the product of two spectroscopic factors, one for the projectile overlap and one for the target overlap; in the case of the ${}^AZ(d,p){}^{A+1}Z$ reaction the $d = n + p$ and the ${}^{A+1}Z = {}^AZ + n$ overlaps, respectively. The spectroscopic factor for the projectile overlap is usually determined by other means, often a nuclear structure calculation.

It is apparent from the foregoing that a model of the reaction process is essential if we wish to obtain nuclear structure information from direct reaction data. In the remainder of these lecture notes we shall concern ourselves with four of the most popular of these models viz., in order of increasing sophistication:

1. The Distorted Wave Born Approximation (DWBA). The simplest useful reaction model, which assumes a direct, one-step transfer process where the transfers to specific states are individually weak and may be treated using perturbation theory.
2. The adiabatic model. A modification of the DWBA specific to (d,p), (d,n), (p,d) and (n,d) reactions that takes effects due to breakup of the weakly-bound deuteron into account in an approximate way.
3. The Coupled Channels Born Approximation (CCBA). Used when the assumption of a one-step transfer process breaks down, it allows for two-step transfer paths including inelastic excitation of the target, projectile or residual nucleus. The strong inelastic excitations are modelled using the coupled channels technique while the DWBA is retained for the weak transfer step.
4. Coupled Reaction Channels (CRC). The most sophisticated readily available model of the transfer process. It does not assume that the transfer is either one-step or weak and all reaction processes are treated on an equal footing. Complex rearrangements of flux between channels are possible, sometimes leading to surprising results.

THE DISTORTED WAVE BORN APPROXIMATION

Despite its simplicity and longevity — it was first developed approximately fifty years ago — the DWBA is still widely used today. What, then, are the basic “ingredients” of a typical DWBA calculation? They fall under two main headings: firstly, we require, at

least in principle, optical model potentials that describe the appropriate elastic scattering in the entrance and exit channels. These potentials are used to provide the distorted waves that give the model its name. However, appropriate elastic scattering data are often unavailable and one is constrained to use global parameterizations, an often far from ideal expedient. Secondly, potentials that bind the transferred particle to the light and heavy “core” nuclei — e.g. for the $^{12}\text{C}(d,p)^{13}\text{C}$ reaction the proton is the light and the ^{12}C the heavy “core” nucleus for the transferred neutron — and the internal wave functions of the composite nuclei thus formed derived from these binding potentials are required. The internal wave functions are usually calculated by binding the transferred particle in a Woods-Saxon potential well of fixed “geometry”, i.e. radius and diffuseness, with a depth adjusted to give the known binding energy of the state in question. This is sometimes referred to as the “well-depth prescription” and obviously needs to be reconsidered if transfer to an unbound resonant state is under consideration.

Some further details are needed to calculate the internal wave functions. In what follows we tacitly assume for the sake of simplicity a (d,p)-type reaction on an even-even target. The necessary information consists of:

1. The spin-parity (J_R^π) of the state of the residual or “composite” nucleus.
2. The angular momentum (L) of the transferred particle relative to the “core” nucleus.
3. The number of nodes (N) in the radial wave function.

These quantities are known for the light interacting partner (the deuteron in a (d,p) reaction, for example) and are sometimes obtained from a theoretical potential, e.g. the Reid soft-core N-N interaction [8] for the $d = n + p$ wave function. For the heavy partner they form part of the spectroscopic information we wish to determine; as we have seen, in general only L is unambiguously determined by the data.

To obtain L from the data we also have to assume a definite J in our calculation, plus a value for N . This is normally done by consulting a shell model scheme or, if possible, a nuclear structure calculation and picking a level that seems to correspond to that observed; N is then the principal quantum number of the selected state (there are complications for the transfer of composite particles such as d , ^3He , ^4He etc. which are covered in the book by Satchler [2]). Two typical radial wave functions obtained using the well-depth prescription are shown in Fig. 5.

After assembling our ingredients we may obtain the spectroscopic factor for each state by normalising our DWBA calculations to the measured angular distributions, having first obtained the correct L values by a careful comparison of the forms of the calculated angular distributions with the measured ones. However, the reality is not quite so simple, as there are a number of ambiguities and traps for the unwary. Firstly, there are ambiguities in the empirical optical model potentials used to calculate the distorted waves in the entrance and exit channels; several different “families” of potentials will often be found that fit the elastic scattering data equally well and the choice of potential will affect both the value obtained for the spectroscopic factor and the shape of the transfer angular distribution. Secondly, the geometry parameters of the binding potentials are rather arbitrary as there is a wide range of “reasonable” values. As the cross section scales with the choice of radius parameter the derived spectroscopic factor can vary by up to 30 % depending on the chosen value. Finally, check the

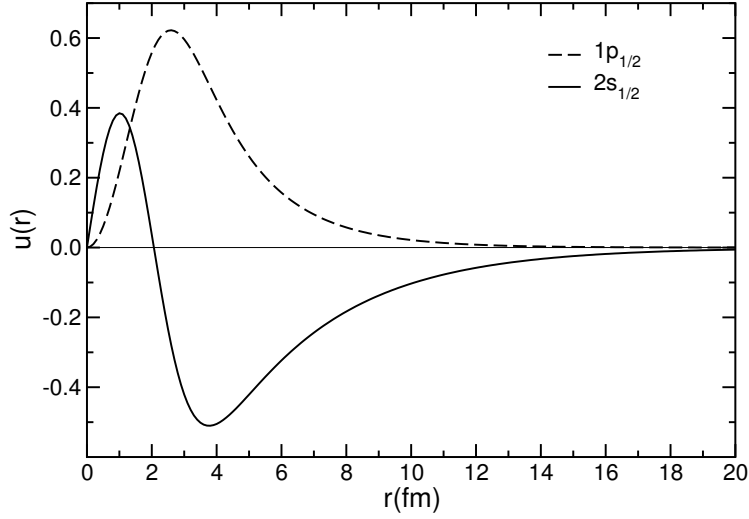


FIGURE 5. Radial wave functions for the $1p_{1/2} 1/2^-$ ground state and $2s_{1/2} 1/2^+$ first excited state of ^{13}C , calculated using the well-depth prescription and binding the neutron to the ^{12}C core in a Woods-Saxon well of radius $1.25 \times 12^{1/3}$ fm and diffuseness 0.65 fm.

definition of N in the code you use — some codes start from $N = 1$, equivalent to counting the node in the radial wave function at $r = 0$ but not that at $r = \infty$, others from $N = 0$, equivalent to not counting either the node at $r = 0$ or $r = \infty$. Again, the cross section scales with the value of N so that an error here will affect the extracted spectroscopic factor.

THE ADIABATIC MODEL

Apart from the effect of ambiguities in the optical model potentials and the binding potential geometry, the DWBA is unable to provide a satisfactory description of the data for many (d,p) and (p,d) reactions for incident energies of around 20 MeV and higher [9]. This problem has been found to be caused by effects due to breakup of the weakly bound deuteron. The adiabatic model [9, 10] takes these effects into account in an approximate way by a redefinition of the incident (for (d,p) reactions) or exit (for (p,d) reactions) deuteron distorted wave — it still describes the motion of the centre of mass of the neutron and proton but they are now no longer necessarily propagating in the form of a bound deuteron. This is achieved in practice by introducing an *adiabatic potential* into a standard DWBA code in place of the usual deuteron optical model potential.

The crucial difference between the DWBA and the adiabatic model is therefore contained in the use of the adiabatic potential, which is formally defined as:

$$\bar{V}(\vec{R}) = D_0^{-1} \int d\vec{r} \left[V_n \left(\vec{R} + \frac{1}{2}\vec{r} \right) + V_p \left(\vec{R} - \frac{1}{2}\vec{r} \right) \right] V_{np} \phi_d(r) \quad (6)$$

where:

$$D_0 = \int d\vec{r} V_{np} \phi_d(r) \quad (7)$$

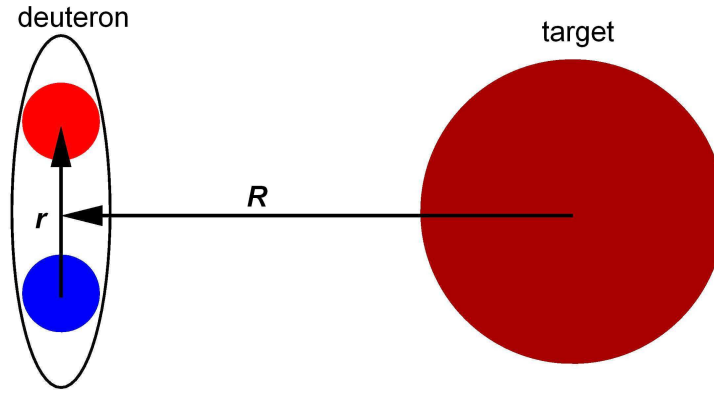


FIGURE 6. Coordinate scheme for calculating the adiabatic potential.

and V_p and V_n are the proton and neutron plus target optical potentials at half the incident deuteron kinetic energy, V_{np} and ϕ_d are the neutron-proton interaction and deuteron internal wave function and \vec{R} and \vec{r} are the radius vectors of the deuteron centre of mass relative to the target and the neutron relative to the proton, see Fig. 6. Approximate relations have been worked out for standard forms of V_p and V_n and the results found to give excellent agreement with those calculated using equation 6, see e.g. Ref. [10].

The use of the adiabatic model can lead to significant improvement in the description of data, see Fig.7, although it should be noted that in this form the adiabatic model will *not* describe the deuteron elastic scattering data — remember that the “deuteron” distorted wave was redefined — although this is possible within the adiabatic model framework [9]. Apart from the substitution of the adiabatic potential for the deuteron optical potential the ingredients of an adiabatic model calculation are the same as for standard DWBA.

THE COUPLED CHANNELS BORN APPROXIMATION

A CCBA calculation proceeds in the same way as for the DWBA with the same ingredients, apart from the following additions: firstly, the inelastic scattering is now modelled explicitly using the coupled channels formalism (see the books by Hodgson [1] and Satchler [2] for details) and requires a Coulomb, $B(E\lambda)$, and a nuclear, β_λ (deformation *parameter*, dimensionless) or δ_λ (deformation *length*, dimensions of length, usually in units of fm), coupling strength where λ is the multipolarity of the inelastic excitation. Secondly, the spectroscopic factors are replaced by spectroscopic *amplitudes*, the square roots of the spectroscopic factors which can have a positive or negative sign — interference effects between two routes to the same final state are now possible. Note that as the inelastic scattering is now explicitly taken into account one must readjust the parameters of the entrance channel optical potential to recover the fit to the elastic scattering data.

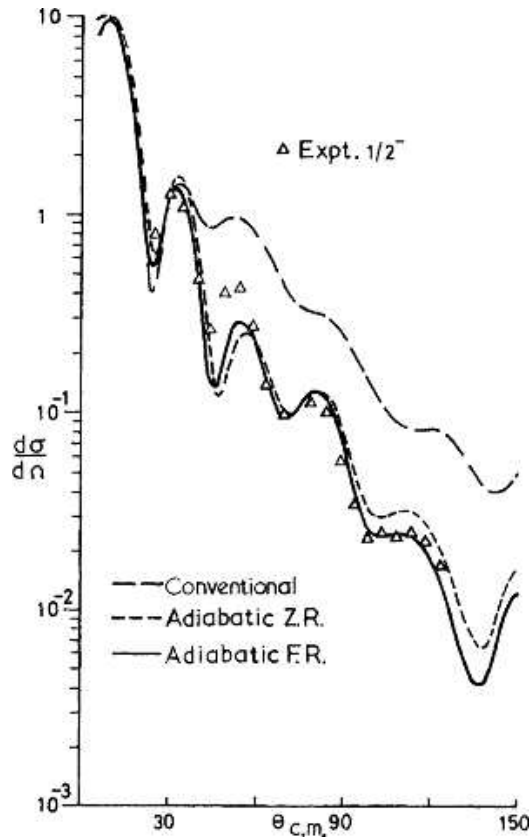


FIGURE 7. Data for the $^{54}\text{Fe}(d,p)^{55}\text{Fe}$ reaction at 23 MeV compared to standard DWBA (Conventional) and two adiabatic model calculations (Adiabatic Z.R. and F.R.). Taken from Ref. [10].

COUPLED REACTION CHANNELS

A coupled reaction channels calculation proceeds as for the CCBA and with the same basic ingredients. However, the transfer couplings will now have an effect on the elastic scattering too — they are no longer modelled using the DWBA — hence further adjustment of the entrance channel optical potential will in general be necessary. There is a further complication, shared with the CCBA, in that for a given state of the residual nucleus there may now be several spectroscopic amplitudes (with their relative signs) to be determined from the same data set in place of the single spectroscopic factor of the DWBA. In practice, one often has to be guided by a nuclear structure calculation of these quantities. Care should be taken to check the “phase convention” between the signs of different bound-state wave functions used in nuclear structure calculations and the direct reaction code used for the analysis. Some reaction codes employ the convention that all radial wave functions are at first positive as r is increased from zero; this is not always the case in nuclear structure calculations and will affect the relative signs between spectroscopic amplitudes. Finally, with CRC one must take account of the non-orthogonality of the entrance and exit channels. This should be corrected for and the correction is often important.

A PRACTICAL EXAMPLE

To illustrate how the above models work in practice we shall take the $^{12}\text{C}(\text{d},\text{p})^{13}\text{C}$ reaction, known as a deuteron stripping reaction as the neutron is “stripped” from the deuteron and transferred to the ^{12}C target, at an incident deuteron energy of 30 MeV. These data will be analysed in turn with progressively more physically sophisticated reaction models and the effect on the extracted spectroscopic factors noted. We shall also illustrate some of the sources of ambiguity in any analysis of direct reaction data, such as choice of distorting optical model potentials and binding potential geometry. The $^{12}\text{C}(\text{d},\text{p})^{13}\text{C}$ transfer data are taken from Ohnuma *et al.* [11], the $^{12}\text{C}(\text{d},\text{d})^{12}\text{C}$ elastic scattering data from Perrin *et al.* [12], the $^{12}\text{C}(\text{d},\text{d}')^{12}\text{C}$ inelastic scattering data to the 4.4 MeV 2^+ state of ^{12}C from Lind *et al.* [13] and finally, the $^{13}\text{C}(\text{p},\text{p})^{13}\text{C}$ elastic scattering data from Greaves *et al.* [14].

We begin with two DWBA analyses with fitted and global optical model potentials. Before we start, our first requirement is a reaction model code. There are many available for DWBA calculations, two popular choices being DWUCK4 and DWUCK5 [15]. However, we shall use the code FRESKO [16], a flexible universal nuclear reaction code which may also be used for CCBA and CRC calculations and which was employed for all the calculations presented here.

Standard DWBA Analyses With Fitted and Global Optical Model Potentials

We present in this section two parallel DWBA analyses of the same $^{12}\text{C}(\text{d},\text{p})^{13}\text{C}$ data set, one employing empirical optical model distorting potentials obtained from fits to the relevant $^{12}\text{C}(\text{d},\text{d})^{12}\text{C}$ and $^{13}\text{C}(\text{p},\text{p})^{13}\text{C}$ elastic scattering data and one employing global deuteron and proton optical model parameter sets. The interest in this comparison arises from the fact that one is often constrained to use global parameter sets when analysing radioactive beam data due to the lack of suitable elastic scattering measurements. As we shall see, even for stable nuclei where the global parameter sets should work reasonably well, this can lead to important differences in the extracted spectroscopic factors.

The fitted optical model potentials for $\text{d} + ^{12}\text{C}$ and $\text{p} + ^{13}\text{C}$ were taken from Perrin *et al.* [12] and a fit to the data of Greaves *et al.* [14], respectively. The global deuteron potential was that of An and Cai [17] while the global proton potential was that of Watson *et al.* [18]. The rest of the basic ingredients were identical for the two sets of calculations. The deuteron internal wave function was calculated using the Reid soft core potential [8] while the ^{13}C internal wave functions were calculated in the well-depth prescription, with the neutron bound to the ^{12}C core in a Woods-Saxon well of radius $1.25 \times 12^{1/3}$ fm and diffuseness 0.65 fm, the well depth being adjusted to give the correct binding energy, plus a spin-orbit potential of the same geometry with a fixed well depth of 6 MeV.

In Figs. 8 and 9 we compare the measured $\text{d} + ^{12}\text{C}$ and $\text{p} + ^{13}\text{C}$ elastic scattering angular distributions with both sets of calculations. While the global parameters give a rather good description of the deuteron elastic scattering, the description of the exit

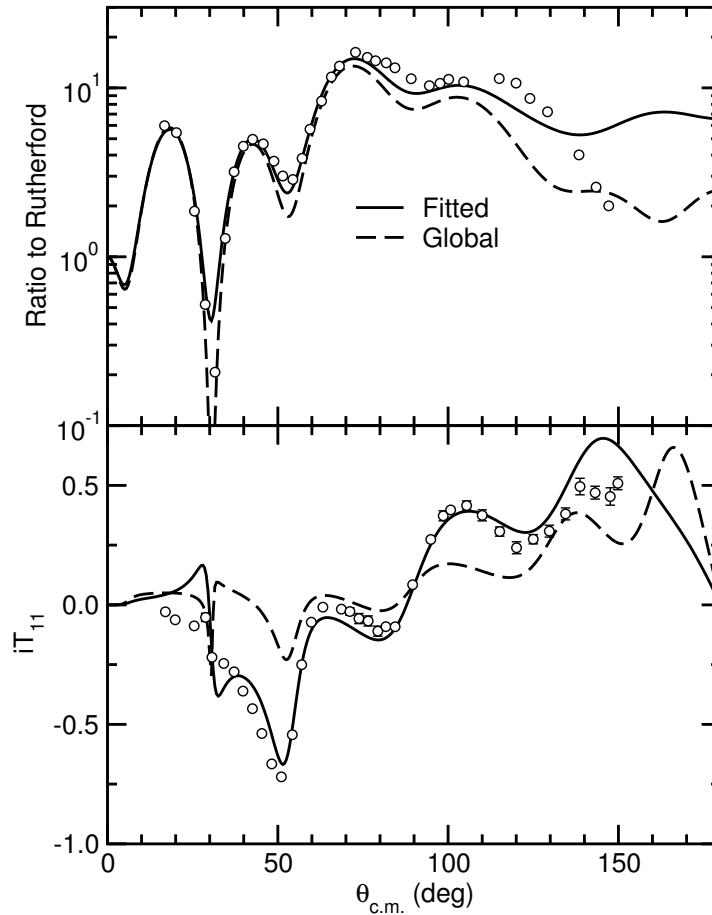


FIGURE 8. Data for 30 MeV $^{12}\text{C}(d,d)^{12}\text{C}$ elastic scattering [12] compared to the optical model calculations using fitted (solid curve) and global (dashed curve) parameters.

channel proton scattering is poor; although the form of the angular distribution is good the absolute magnitude is too large. The description of the vector analysing powers by the global potentials is reasonable for both data sets. We therefore see that the use of a global parameter set violates one of the basic tenets of the DWBA, i.e. that the distorting potentials should reproduce the appropriate elastic scattering, as far as the exit channel is concerned. The effect of this will become apparent when we compare the two sets of calculations for the (d,p) transfer.

The (d,p) transfer data to the 0.0 MeV $1/2^-$, 3.09 MeV $1/2^+$ and 3.85 MeV $5/2^+$ states in ^{13}C are compared to the two sets of calculations in Figs. 10-12. For the purposes of this example transfers to states of known spin-parity are considered. Taking each transfer in turn, we see that for the 0.0 MeV $1/2^-$ state both calculations produce cross section angular distributions of similar form, that employing the global potentials giving a slightly better overall description of the data. However, neither calculation can be said to provide a satisfactory fit to the data as they both fall off much too rapidly with scattering angle compared to the measured angular distribution. For the transfer leading to the 3.09 MeV $1/2^+$ state, although both calculated angular distributions exhibit the

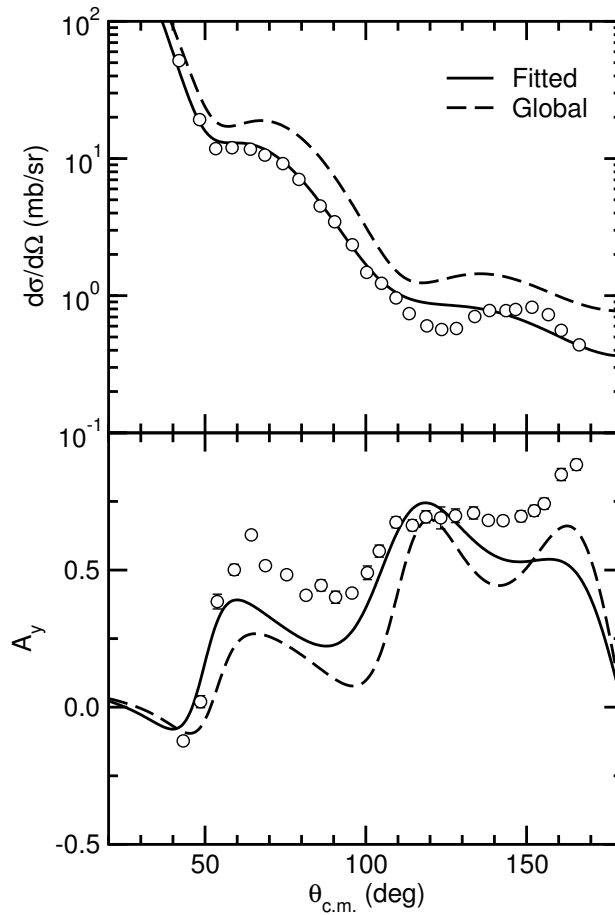


FIGURE 9. Data for 30 MeV $^{13}\text{C}(p,p)^{13}\text{C}$ elastic scattering [14] compared to the optical model calculations using fitted (solid curve) and global (dashed curve) parameters.

characteristic form of an $L = 0$ transfer neither provides a satisfactory description of the data. There is a significant angle phase error in the position of the first minimum of the angular distribution for both calculations, worst for the global potentials. This phase error is also characteristic of many $L = 0$ DWBA calculations! The magnitude of the second peak in the angular distribution relative to that at 0° is also too large in the calculations compared to the data, the calculation using the global potentials again being much worse in this respect. Finally, for transfer leading to the 3.85 MeV $5/2^+$ state both calculations give identical angular distributions, providing a good description of the data out to about 30° . Thereafter the calculated cross sections are too large compared to the data. Although there are no data available, calculated vector analysing power angular distributions are also given in Figs. 10-12 for the sake of completeness. The results of the two calculations are not significantly different.

The spectroscopic factors extracted from the two sets of calculations are given in Table 1. Spectroscopic factors were obtained by normalising the calculated angular distributions to the most forward angle data points, in general good practice as it is in this angular region that the DWBA hypothesis of a direct, one-step transfer mechanism

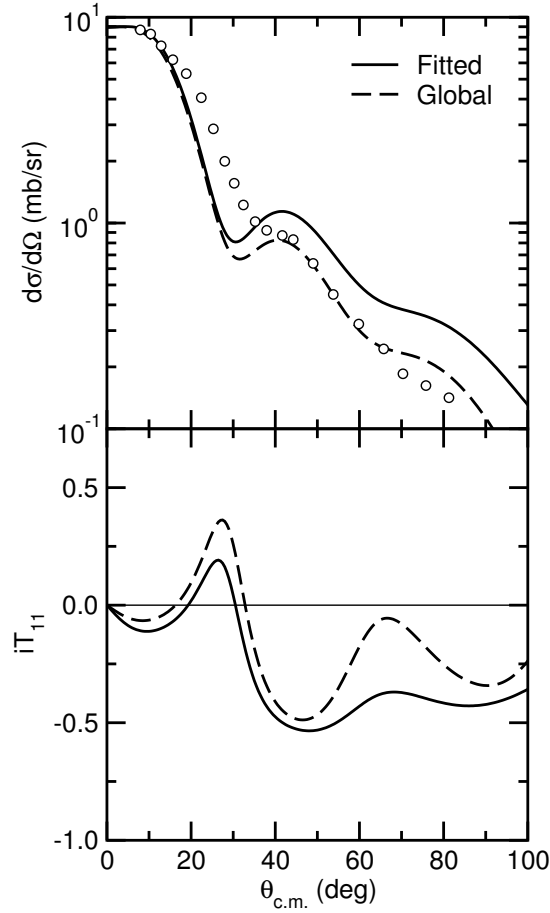


FIGURE 10. Data for the 30 MeV $^{12}\text{C}(d,p)^{13}\text{C}$ transfer to the 0.0 MeV $1/2^-$ state in ^{13}C [11] compared to DWBA calculations using fitted (solid curve) and global (dashed curve) parameters.

TABLE 1. Spectroscopic factors obtained from the two DWBA analyses.

	$1/2^-$	$1/2^+$	$5/2^+$
Fitted potentials	0.76	1.00	0.77
Global potentials	0.62	1.69	0.69

is expected to be most realistic. The spectroscopic factors from the DWBA analysis using global potentials are about 20 % smaller, 70 % larger and 10 % smaller than those obtained from the analysis using fitted potentials for the $1/2^-$, $1/2^+$ and $5/2^+$ states, respectively. The much larger discrepancy for the $1/2^+$ state is due to the significant phase error in the calculated versus measured angular distribution which complicates the normalisation of theory to data.

In summary, the agreement of either set of calculations with the data is poor. Using different fitted optical model potentials does not change this. In addition, it is apparent that the use of global optical model parameter sets, even for stable nuclei, can lead to

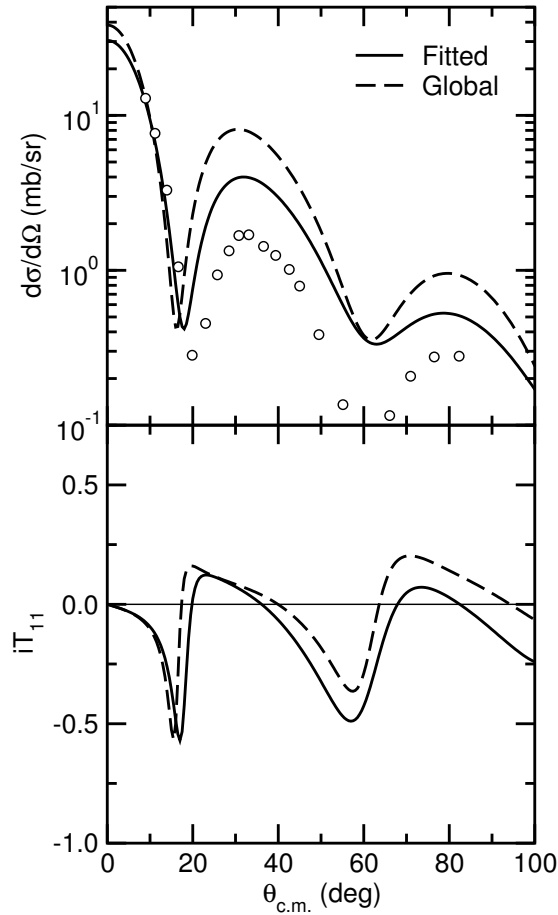


FIGURE 11. Data for the 30 MeV $^{12}\text{C}(d,p)^{13}\text{C}$ transfer to the 3.09 MeV $1/2^+$ state in ^{13}C [11] compared to DWBA calculations using fitted (solid curve) and global (dashed curve) parameters.

important differences in the extracted spectroscopic factors. The poor agreement with the data suggests that the DWBA, with its underlying assumptions that the individual transfers are weak and thus possible to treat within the framework of perturbation theory and proceed in a single step, is not an adequate model of the reaction process in this case.

As ^{12}C has a strongly coupled first excited state, the 4.4 MeV 2^+ , could a CCBA calculation including transfer paths where the stripped neutron is attached to the ^{12}C core in its excited state as well as the ground state improve the description of the data? This possibility will be investigated in the next section.

CCBA Analysis

As the DWBA has proved inadequate to describe these data we now present a CCBA analysis where coupling to the ^{12}C 4.4 MeV 2^+ state is explicitly taken into account, allowing additional transfer paths via this state. As stated above, Coulomb and nuclear

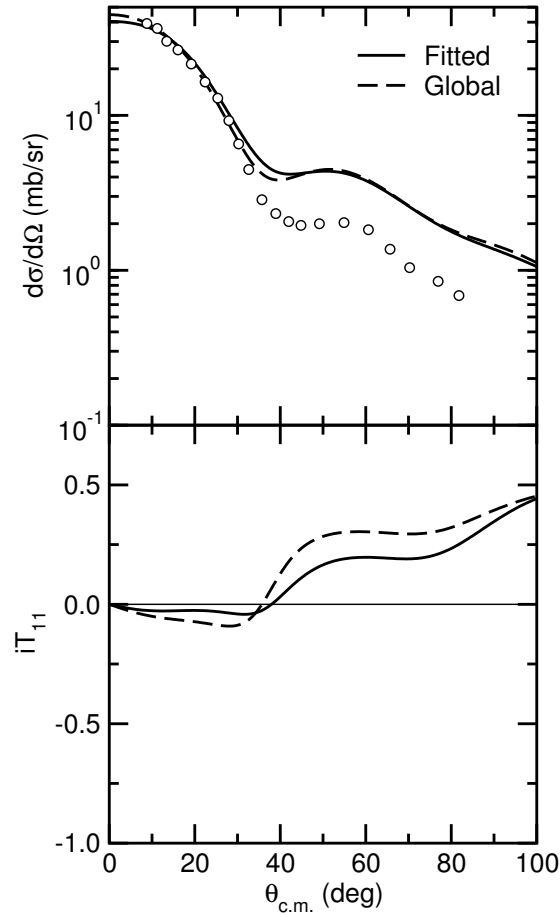


FIGURE 12. Data for the 30 MeV $^{12}\text{C}(d,p)^{13}\text{C}$ transfer to the 3.85 MeV $5/2^+$ state in ^{13}C [11] compared to DWBA calculations using fitted (solid curve) and global (dashed curve) parameters.

coupling strengths are required for the inelastic scattering. For the Coulomb coupling strength we took the recommended value for the $B(E2; 0^+ \rightarrow 2^+)$ from the compilation of Raman *et al.* [19]. The nuclear coupling strength, in this case the deformation length δ_2 , was extracted from the $B(E2)$ value assuming the collective model; this simplifying assumption will obviously need to be re-examined for exotic nuclei where the neutron and proton densities may be very different. The fitted optical model potentials used in the DWBA analysis were retained but the parameters of the entrance channel deuteron potential were readjusted to recover the fit to the elastic scattering data.

In Figs. 13 and 14 the calculated deuteron elastic and inelastic scattering angular distributions are compared with the data. Apart from a slight deterioration in the description of the analysing power (the spin-orbit component of the deuteron optical potential was not adjusted) the agreement with the elastic scattering data is as good as for the optical model fit. The agreement with the inelastic scattering data, while not perfect, is acceptable.

The CCBA does not significantly improve the agreement with the transfer data, except for transfer to the 3.09 MeV $1/2^+$ state. The angular distributions for both cross section

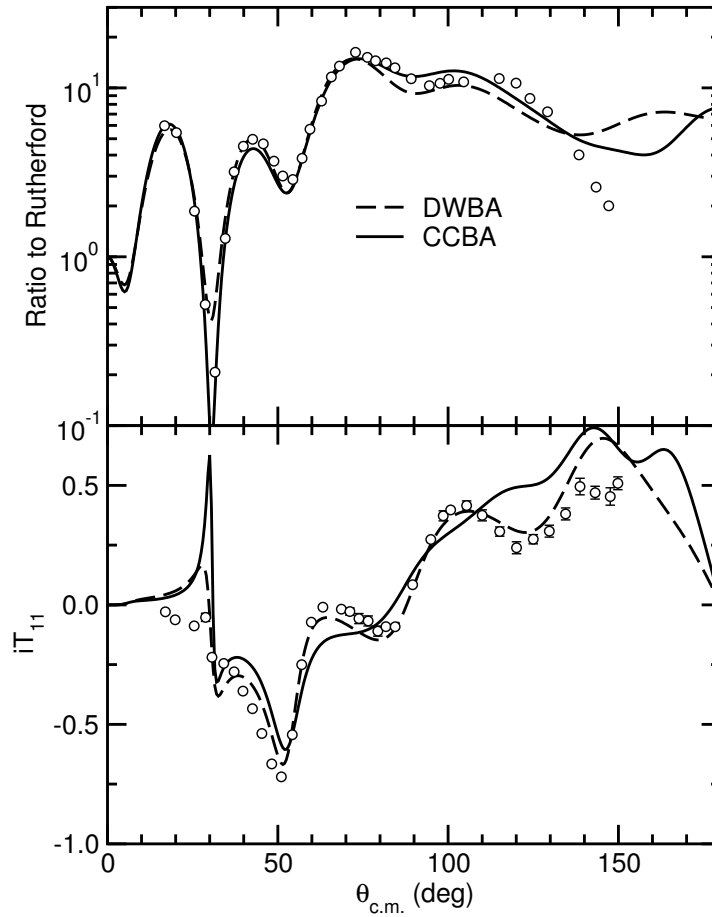


FIGURE 13. Data for 30 MeV $^{12}\text{C}(d,d)^{12}\text{C}$ elastic scattering [12] compared to the CCBA calculation (solid curve). The optical model calculation with fitted potential parameters is also given for comparison (dashed curve).

and vector analysing power for transfer to the 0.0 MeV $1/2^-$ and 3.85 MeV $5/2^+$ states are identical to those obtained with the DWBA and will not be shown here. However, the extra transfer path via the ^{12}C 4.4 MeV 2^+ state does significantly improve the fit to the $1/2^+$ state data, moving the first minimum to match the data, see Fig. 15.

The main effect of the additional transfer paths available within the CCBA framework is to change the spectroscopic factors somewhat compared to the DWBA analysis. The CCBA analysis yields spectroscopic *amplitudes* rather than factors, as stated above, but these are merely the square roots of the spectroscopic factors. The values obtained in the current analysis are given in Table 2; the symbol “ \otimes ” denotes “is coupled to.” Squaring the values given in the first row of Table 2 we obtain the following spectroscopic factors for the transferred neutron coupled to the ^{12}C core in its ground state: 0.90, 0.83 and 0.81 for transfer to the ^{13}C $1/2^-$, $1/2^+$ and $5/2^+$ states, respectively. These may be directly compared to the values obtained in the DWBA analysis using fitted potentials: 0.76, 1.0 and 0.77, showing an increase of about 18 %, a decrease of about 17 % and an increase of about 5 %, respectively for the CCBA over the DWBA values.

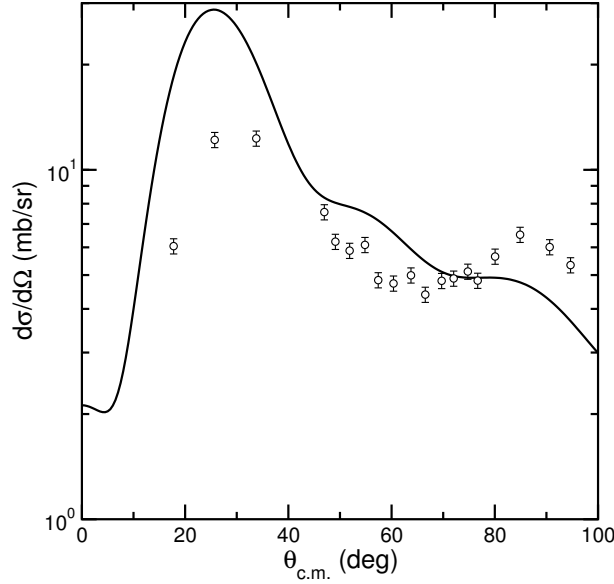


FIGURE 14. Data for 30 MeV $^{12}\text{C}(d,d')^{12}\text{C}$ inelastic scattering to the 4.4 MeV 2^+ state [13] compared to the CCBA calculation (solid curve).

TABLE 2. Spectroscopic amplitudes determined from the CCBA analysis. The left-hand column denotes the ^{12}C core spin and the ℓ, j quantum numbers of the transferred neutron.

Configuration	$\frac{1}{2}^-$	$\frac{1}{2}^+$	$\frac{5}{2}^+$
$0 \otimes j$	0.95	0.91	0.90
$2 \otimes s_{1/2}$	—	—	0.70
$2 \otimes p_{3/2}$	-0.40	—	—
$2 \otimes d_{5/2}$	—	-0.40	-0.30

In summary, with the exception of transfer to the 3.09 MeV $1/2^+$ state, CCBA does not improve the agreement between calculations and data. Nevertheless, even though the angular distributions for transfer to the 0.0 MeV $1/2^-$ and 3.85 MeV $5/2^+$ state calculated with the CCBA are essentially identical to those calculated with the DWBA the extracted spectroscopic factors can be significantly different. The main success of the CCBA over the DWBA in this case is that it can eliminate the angle phase error in the calculated angular distribution for the $1/2^+$ state, considerably improving the description of the data. It should be noted, however, that in general the spectroscopic amplitudes for the two-step transfer paths via the ^{12}C 2^+ excited state are not well determined by the data. Transfer to the $1/2^+$ state again forms an exception, as the position of the first minimum in the angular distribution enables the $^{12}\text{C}(2^+) \otimes p_{3/2}$ spectroscopic amplitude to be rather accurately fixed. Overall, we see that the CCBA does not solve all our problems and that we must consider other influences such as the effect due to breakup of the deuteron. These will be investigated in the next two sections, firstly using the approximate adiabatic model then using a more sophisticated coupled-

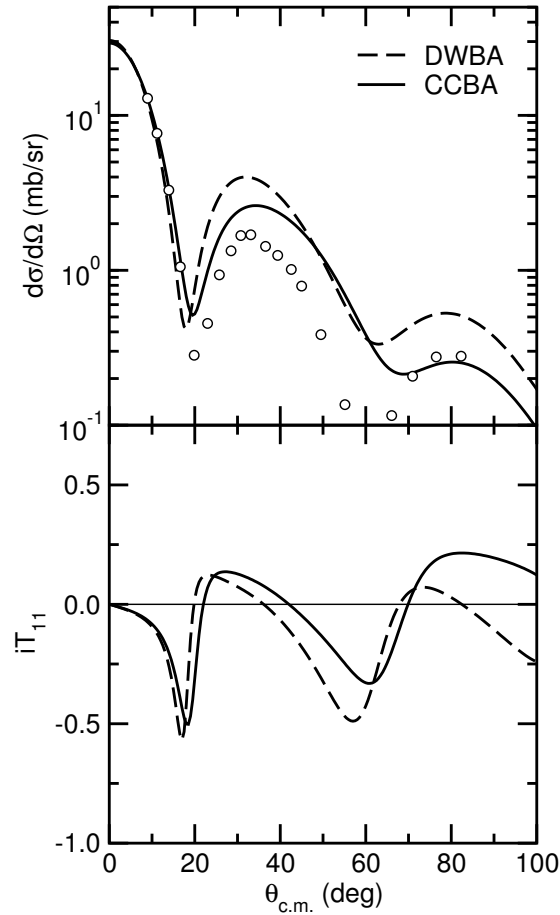


FIGURE 15. Data for the 30 MeV $^{12}\text{C}(\text{d},\text{p})^{13}\text{C}$ transfer to the 3.09 MeV $1/2^+$ state in ^{13}C [11] compared to the CCBA calculation (solid curve). The DWBA calculation with fitted potential parameters is also given for comparison (dashed curve).

channels based model.

Breakup Effects (1): The Adiabatic Model

We shall first consider the influence of deuteron breakup on the $^{12}\text{C}(\text{d},\text{p})^{13}\text{C}$ transfer reaction by employing the adiabatic model, discussed previously. This model has not yet been formulated to allow inelastic excitation of the target to be taken into account consistently so we shall only consider one-step transfer, as in the DWBA. The potentials V_p and V_n , required to calculate the adiabatic deuteron potential, were taken from optical model fits to $\text{p} + ^{12}\text{C}$ [20] and $\text{n} + ^{12}\text{C}$ [21] elastic scattering data at an incident energy of 15 MeV. All other details were as for the DWBA calculation using fitted optical potentials.

We present the results of the transfer calculations using the adiabatic model in Figs. 16-18 (it will be recalled that a comparison with the deuteron elastic scattering is not

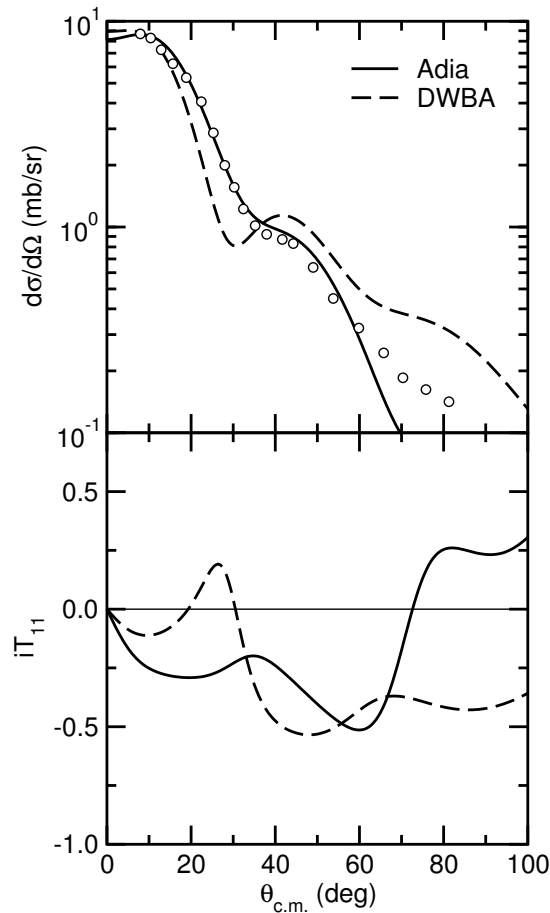


FIGURE 16. Data for the 30 MeV $^{12}\text{C}(d,p)^{13}\text{C}$ transfer to the 0.0 MeV $1/2^-$ state in ^{13}C [11] compared to the adiabatic model calculation (solid curve) with the DWBA calculation using fitted parameters given for comparison (dashed curve).

relevant for the adiabatic model in this form). Taking each transfer in turn, we see that for transfer leading to the 0.0 MeV $1/2^-$ state in ^{13}C the adiabatic model description is considerably improved compared to that of the DWBA, providing a good fit over almost the entire angular range of the data. Note also the significant effect on the vector analysing power. For transfer leading to the 3.09 MeV $1/2^+$ state in ^{13}C the adiabatic model fit is perhaps slightly better overall than that of the DWBA, although the position of the first minimum in the angular distribution is now shifted to slightly too large an angle. Again, note the significant effect on the analysing power. Finally, for transfer leading to the 3.85 MeV $5/2^+$ state the overall fit to the data is better than for the DWBA, although at angles $\theta < 30^\circ$ the slope of the adiabatic model calculation is not steep enough compared to the data, unlike the DWBA result. The effect on the analysing power is much less marked than for the two other transfers.

The most important effect of the adiabatic model is, however, on the spectroscopic factors. These are: 0.38, 0.41 and 0.52 for transfer to the $1/2^-$, $1/2^+$ and $5/2^+$ states of ^{13}C , respectively and correspond to reductions of about 50 %, 59 % and 32 % compared

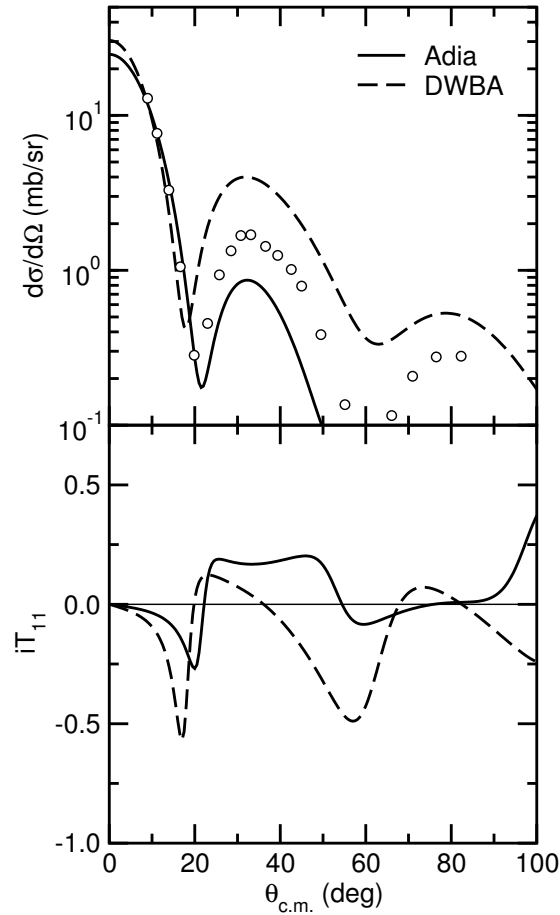


FIGURE 17. Data for the 30 MeV $^{12}\text{C}(d,p)^{13}\text{C}$ transfer to the 3.09 MeV $1/2^+$ state in ^{13}C [11] compared to the adiabatic model calculation (solid curve) with the DWBA calculation using fitted parameters given for comparison (dashed curve).

to the values obtained with the DWBA using fitted potentials.

In summary, it is apparent that the adiabatic model gives much improved overall agreement with the transfer data compared to either the DWBA or CCBA analyses. The most striking improvement is in the fit to the data for transfer leading to the 0.0 MeV $1/2^-$ state in ^{13}C . There are also important effects on the vector analysing powers, although the most dramatic influence is on the spectroscopic factors which are substantially reduced compared to those obtained using the DWBA.

Breakup Effects (2): CDCC/CRC calculations

As stated above, the adiabatic model is an approximate treatment of the effects due to deuteron breakup in (d,p) and (p,d) reactions. A more sophisticated approach known as the coupled discretised continuum channels (CDCC) method [22] is available and may be combined with CRC, used to model the transfer steps, to give the most complete

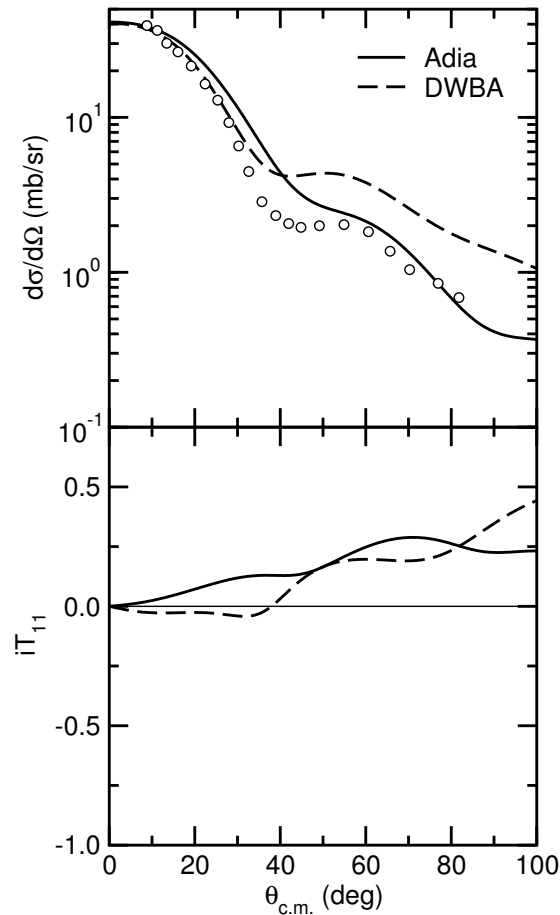


FIGURE 18. Data for the 30 MeV $^{12}\text{C}(d,p)^{13}\text{C}$ transfer to the 3.85 MeV $5/2^+$ state in ^{13}C [11] compared to the adiabatic model calculation (solid curve) with the DWBA calculation using fitted parameters given for comparison (dashed curve).

calculation of such reactions that we are able to perform at the present time. We shall not give details of the method here as it is beyond the scope of these lectures and will merely present the results. Couplings to deuteron breakup, inelastic excitation of the ^{12}C 4.4 MeV 2^+ state and transfer paths via both the 0^+ ground and 2^+ excited states of ^{12}C were included in the calculation that follows. The correction due to the non-orthogonality of the wave functions in the entrance and exit channels was also included.

In Figs. 19 and 20 the calculated deuteron elastic and inelastic scattering angular distributions are compared with the data. The description of the elastic scattering cross section data is comparable to that of the optical model fit; the poor description of the vector analysing power is due to the absence of a static spin-orbit potential, known to dominate iT_{11} for deuteron elastic scattering, due to limitations in the code FRESKO. It is not significant for the fit to the transfer data, as will be seen below. The inelastic scattering to the ^{12}C 4.4 MeV 2^+ state is well described.

The results of the transfer calculations using the CDCC/CRC model are compared with the data in Figs. 21-23 Agreement between calculation and experiment is now very

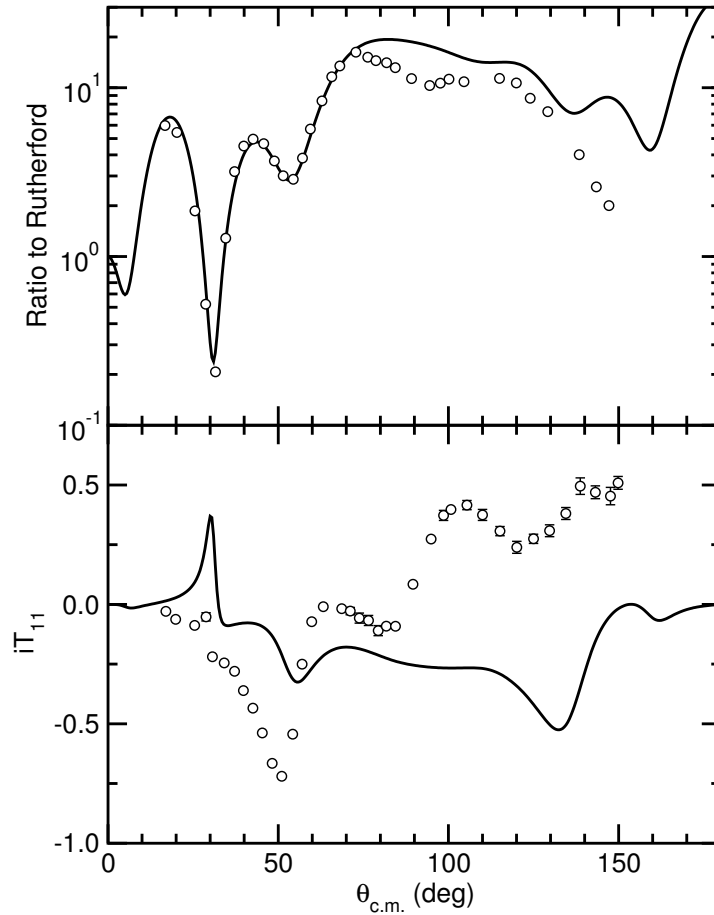


FIGURE 19. Data for 30 MeV $^{12}\text{C}(d,d)^{12}\text{C}$ elastic scattering [12] compared to the CDCC/CRC calculation (solid curve).

TABLE 3. Spectroscopic amplitudes obtained in the CDCC/CRC analysis. The left-hand column denotes the ^{12}C core spin and the ℓ, j quantum numbers of the transferred neutron.

Configuration	$\frac{1}{2}^-$	$\frac{1}{2}^+$	$\frac{5}{2}^+$
$0 \otimes j$	0.81	0.77	0.85
$2 \otimes s_{1/2}$	—	—	0.80
$2 \otimes p_{3/2}$	0.60	—	—
$2 \otimes d_{5/2}$	—	-0.35	0.70

good for the 0.0 MeV $1/2^-$ and 3.09 MeV $1/2^+$ states; the description of the transfer to the 3.85 MeV $5/2^+$ state is similar to that obtained with the DWBA or CCBA. Effects on the calculated vector analysing powers are only important for the 0.0 MeV $1/2^-$ state. The spectroscopic amplitudes obtained are given in Table 3.

In summary, we find that the CDCC/CRC combination provides by far the best overall description of the data, much better than either the DWBA or CCBA. Nevertheless, it

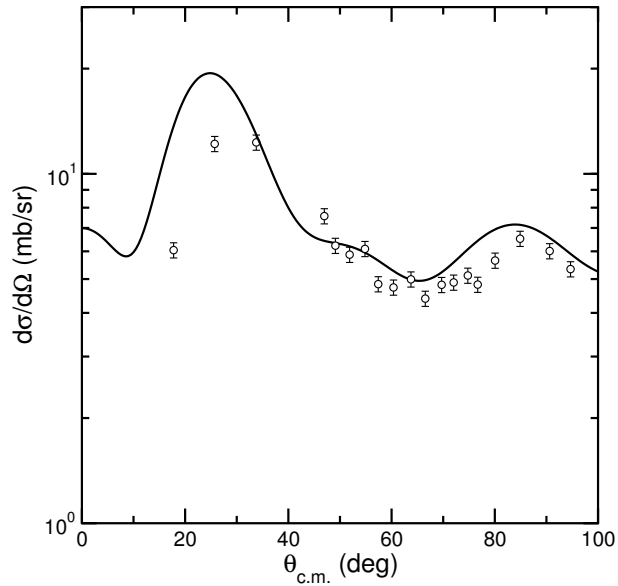


FIGURE 20. Data for 30 MeV $^{12}\text{C}(d,d')^{12}\text{C}$ inelastic scattering to the 4.4 MeV 2^+ state [13] compared to the CDCC/CRC calculation (solid curve).

does not solve the problem of the relatively poor description of the 3.85 MeV $5/2^+$ data. We have also seen how the choice of reaction model can have a significant effect on the shape of the calculated angular distribution, particularly so in this case for the 0.0 MeV $1/2^-$ state. Based on the DWBA or CCBA calculations this state would probably have been given an $L = 2$ assignment rather than $L = 1$ if the actual spin-parity were unknown. It was necessary to take effects due to breakup of the deuteron into account in the analysis, either approximately via the adiabatic model or explicitly through the CDCC formalism to obtain a good description of this state with the correct spin-parity assignment.

Squaring the values given in the first row of Table 3, as was done for the CCBA analysis, we may compare the spectroscopic factors obtained from the CDCC/CRC analysis with those extracted from the DWBA analysis using fitted optical potentials. We obtain values of $C^2S = 0.66, 0.59$ and 0.72 for the ^{13}C 0.0 MeV $1/2^-$, 3.09 MeV $1/2^+$ and 3.85 MeV $5/2^+$ states, respectively, representing reductions of 13 %, 41 % and 6 %. We therefore find that in this case more accurate modelling of deuteron breakup effects with the CDCC formalism leads to much smaller reductions in the extracted spectroscopic factors compared to the DWBA than the approximate treatment of the adiabatic model.

OTHER INFLUENCES ON EXTRACTED SPECTROSCOPIC FACTORS

We saw in the previous section that the choice of reaction model can significantly influence the value obtained for a spectroscopic factor extracted from an analysis of

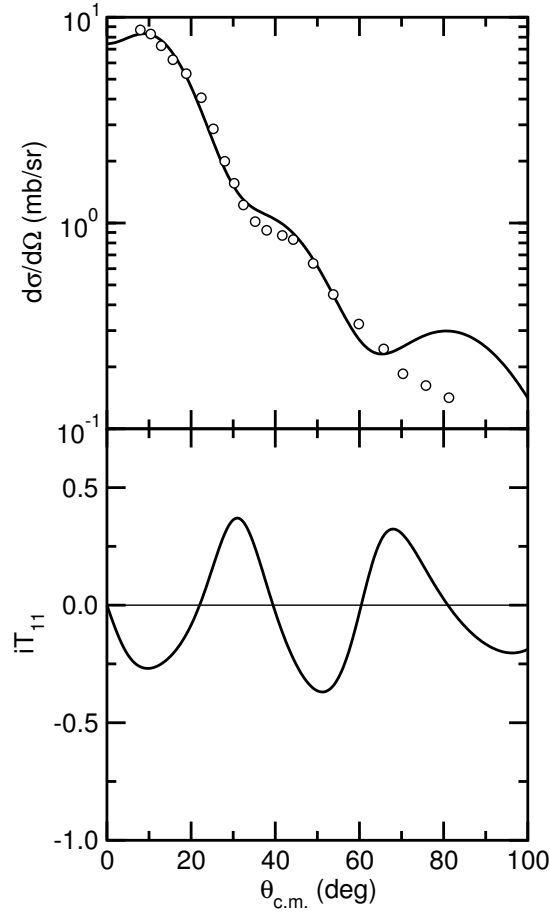


FIGURE 21. Data for the 30 MeV $^{12}\text{C}(d,p)^{13}\text{C}$ transfer to the 0.0 MeV $1/2^-$ state in ^{13}C [11] compared to the CDCC/CRC model calculation.

direct reaction angular distribution data. However, the difference between the simplest useful model (DWBA) and the most sophisticated (CDCC/CRC) was only important for the $L = 0$ transfer in our $^{12}\text{C}(d,p)^{13}\text{C}$ test case. Perhaps the most important influence on the extracted spectroscopic factor is the choice of radius for the Woods-Saxon potential well that binds the transferred particle to the heavy core nucleus (^{12}C in our example). This is the main weakness of the well-depth prescription.

In all the calculations presented so far we have used the parameters: $R_0 = 1.25 \times A^{1/3}$ fm, $a_0 = 0.65$ fm, often regarded as “standard”, although with little real justification. This choice of parameters has a certain sanctity due to its age — it became popular in the 1960s and is derived from an early global proton scattering optical potential — but other choices are equally physically reasonable. In this section we present a series of DWBA calculations for the $^{12}\text{C}(d,p)^{13}\text{C}$ transfer to the 0.0 MeV $1/2^-$ state with different reasonable choices of r_0 ranging from 1.1 to 1.4 fm to demonstrate the effect of this choice on the extracted spectroscopic factor.

In Fig. 24 we present the results of the calculations. Note that the effect on the calculated vector analysing power is negligible. The effect on the cross section angular

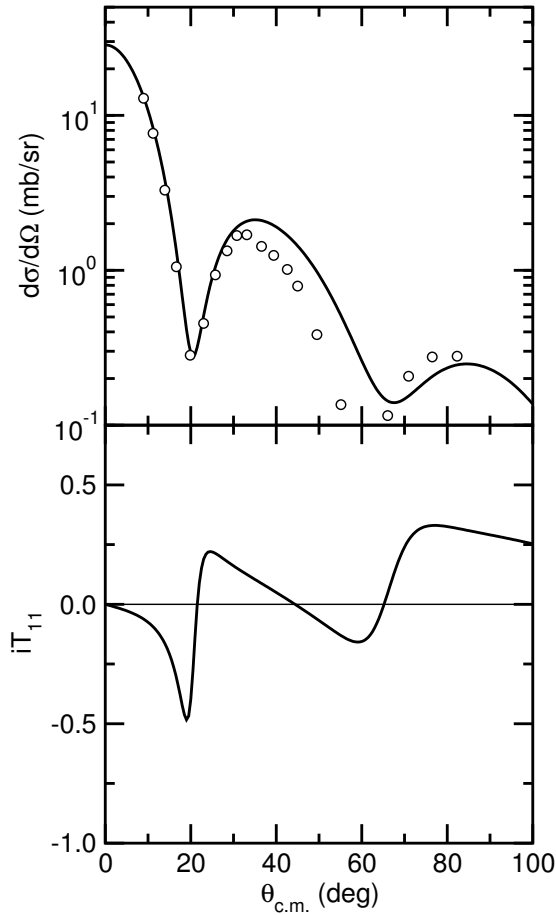


FIGURE 22. Data for the 30 MeV $^{12}\text{C}(\text{d},\text{p})^{13}\text{C}$ transfer to the 3.09 MeV $1/2^+$ state in ^{13}C [11] compared to the CDCC/CRC model calculation.

distribution is only significant for angles greater than about 30° in the centre of mass frame, part of the reason why it is good practice to extract the spectroscopic factor by normalising the calculated angular distribution to the data at forward angles. The most important effect is on the extracted spectroscopic factor, which varies from $C^2S = 0.92$ for $r_0 = 1.1$ fm to $C^2S = 0.61$ for $r_0 = 1.4$ fm, a reduction of $\sim 34\%$. The effect on the extracted spectroscopic factor is much smaller for the $L = 0$ transfer to the 3.09 MeV $1/2^+$ state, C^2S ranging from 1.10 for $r_0 = 1.1$ fm to 0.90 for $r_0 = 1.4$ fm, a reduction of $\sim 18\%$. For the $L = 2$ transfer to the 3.85 MeV $5/2^+$ state the effect is the same as for $L = 1$, C^2S ranging from 0.96 for $r_0 = 1.1$ fm to 0.62 for $r_0 = 1.4$ fm, a reduction of $\sim 35\%$.

SUMMARY SO FAR

We have seen that both choice of reaction model and binding potential well radius can have important effects on the spectroscopic factors extracted from analyses of direct

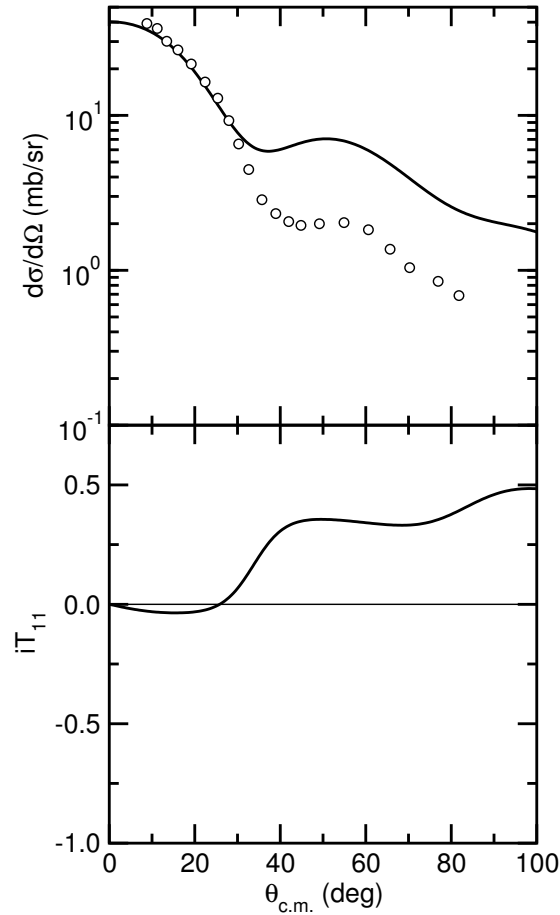


FIGURE 23. Data for the 30 MeV $^{12}\text{C}(d,p)^{13}\text{C}$ transfer to the 3.85 MeV $5/2^+$ state in ^{13}C [11] compared to the CDCC/CRC model calculation.

reaction data, with the latter being, in general, more important. All things considered, an uncertainty of the order of $\pm 30\%$ in the value of an *absolute* spectroscopic factor is not unreasonable — it could be even larger, as this is without taking into consideration uncertainties in the data. These are often quite large ($\pm 20\%$) for radioactive beam data. However, *relative* spectroscopic factors between states of the same nucleus are usually rather better determined, i.e. they are less sensitive to the details of the calculation.

Choosing a more sophisticated reaction model will not only lead to different (and we hope more reliable) spectroscopic factors but will also usually provide a better description of the shape of the angular distribution, thus facilitating the extraction of the spectroscopic factor and giving a more reliable determination of the transferred L value. This is particularly true if the angular coverage of the data is sparse and does not extend very far towards $\theta = 0^\circ$, as is often the case with radioactive beam data.

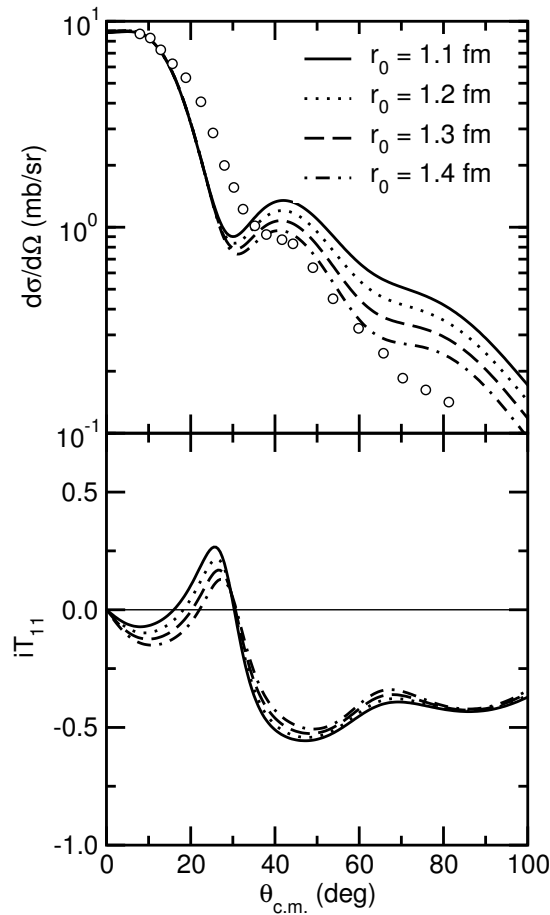


FIGURE 24. DWBA calculations for the $^{12}\text{C}(d,p)^{13}\text{C}$ reaction leading to the 0.0 MeV $1/2^-$ state for various choices of r_0 .

CHOICE OF REACTION MODEL: WHEN IS THE DWBA APPROPRIATE?

We have seen that the DWBA was not adequate to describe the data for the $^{12}\text{C}(d,p)^{13}\text{C}$ reaction at an incident deuteron energy of 30 MeV. However, DWBA remains a useful analysis tool *provided* the tenets of the theory are not violated. As a general rule, staying with (d,p) reactions, the DWBA is an appropriate reaction model for systems with heavy targets at low incident deuteron energies; exactly what constitutes “heavy” and “low” is a rather subjective choice. As a concrete example of a system where the DWBA and the CDCC/CRC method give identical results we take the $^{124}\text{Sn}(d,p)^{125}\text{Sn}$ reaction at an incident deuteron energy of 9 MeV.

The data are taken from Ref. [23] and were actually taken in inverse kinematics with a ^{124}Sn beam. The original DWBA analysis was repeated and a CDCC/CRC calculation was then performed, taking care to reproduce the $^{124}\text{Sn}(d,d)$ elastic scattering predicted by the entrance channel optical potential used in the DWBA analysis. All other input to the CDCC/CRC calculation was as for the DWBA.

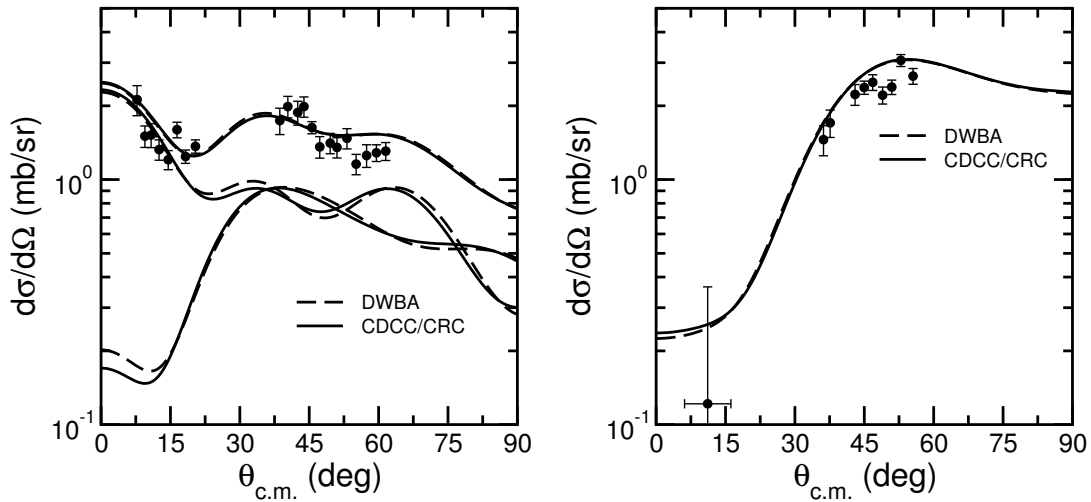


FIGURE 25. DWBA and CDCC/CRC calculations for the $^{124}\text{Sn}(d,p)^{125}\text{Sn}$ reaction at an incident deuteron energy of 9 MeV. The left-hand plot shows data for a single peak combining the 0.0 MeV $11/2^-$, 0.028 MeV $3/2^+$ and 0.215 MeV $1/2^+$ states of ^{125}Sn while the right-hand plot presents data for the 2.8 MeV $7/2^-$ state of ^{125}Sn . Note that the calculations presented in the left-hand plot omit the 0.0 MeV $11/2^-$ state which makes a negligible contribution for angles less than 60° in the centre of mass frame. Data taken from Ref. [23].

We compare the DWBA and CDCC/CRC calculations with each other and the data in Fig. 25. The data consist of angular distributions for two peaks, one combining the 0.0 MeV $11/2^-$, 0.028 MeV $3/2^+$ and 0.215 MeV $1/2^+$ states of ^{125}Sn and one containing the 2.8 MeV $7/2^-$ state of ^{125}Sn only. In the calculations, transfer to the 0.0 MeV $11/2^-$ was omitted, as the contribution of this state for angles smaller than 60° in the centre of mass frame is negligible. The left-hand plot in Fig. 25 shows angular distributions for transfer to the 0.028 MeV $3/2^+$ state, peaked at approximately 40° , the 0.215 MeV $1/2^+$ state, peaked at 0° , and their sum. The right-hand plot shows angular distributions for transfer to the 2.8 MeV $7/2^-$ state. We see that the DWBA and CDCC/CRC calculations give identical results, *provided that the CDCC/CRC calculation reproduces the same entrance channel elastic scattering as the optical model potential used in the DWBA calculation.*

A COUNTER EXAMPLE: A SYSTEM WHERE THE DWBA IS COMPLETELY UNSUITABLE

We have seen in the previous section that the DWBA is able to provide a reliable description of direct reaction data when the basic conditions underlying the theory are fulfilled. However, for systems where one or more of these conditions are violated the use of the DWBA to extract spectroscopic information can give completely misleading results. As an example of such a system we take the $^8\text{He}(p,t)^6\text{He}$ reaction.

Data for this reaction are available at two widely spaced incident energies: 15.7 A.MeV [24] and 61.3 A.MeV [25]. The coupling to the intermediate $^8\text{He}(p,d)^7\text{He}$

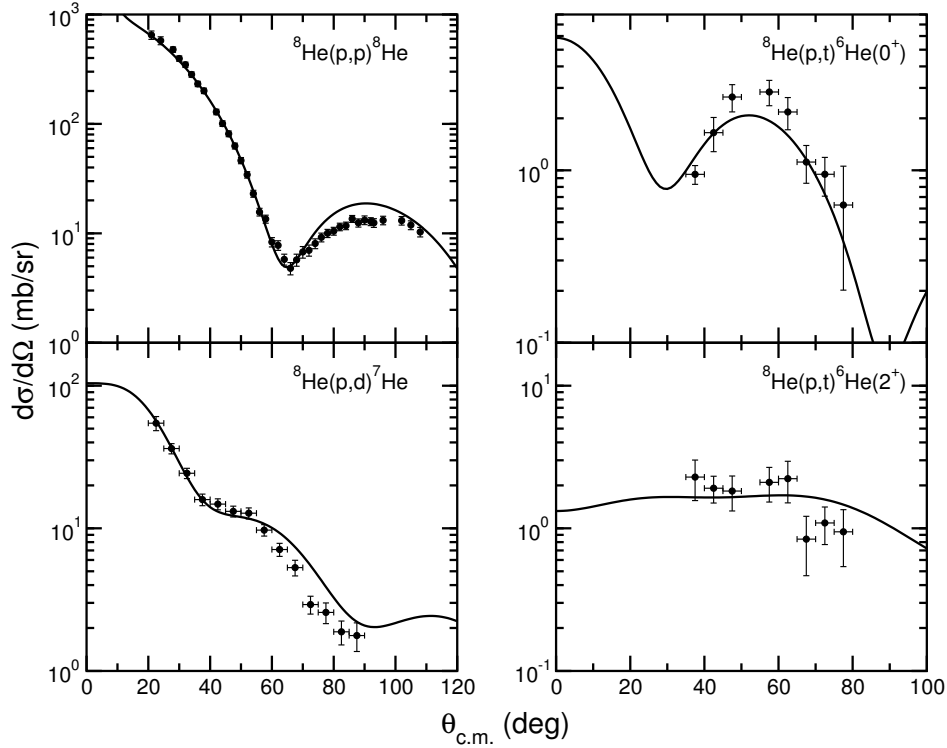


FIGURE 26. Results of the CDCC/CRC calculation for the ${}^8\text{He}(p,t){}^6\text{He}$ reaction at 15.7 A.MeV. The data are taken from [24].

channel is very strong [26] and thus violates two of the basic assumptions underlying the DWBA. The CDCC/CRC combination including the two-step mechanism via the ${}^8\text{He}(p,d){}^7\text{He}(d,t){}^6\text{He}$ process is able to provide a coherent picture of all these data; a DWBA analysis is unable to do so. The results of the CDCC/CRC calculations are compared with the data in Figs. 26 and 27.

It should be noted that both calculations use exactly the same set of spectroscopic amplitudes. The description of the whole data set is good, allowing for the relatively poor quality of the data at 61.3 A.MeV. A DWBA analysis is unable to obtain a consistent description of both data sets with the same spectroscopic factors at both energies, illustrating the importance of accurate modelling of the reaction mechanism. In this case the reaction is no longer a simple direct, one-step transfer.

SUMMARY

We have seen how the choice of reaction model can significantly influence the nuclear structure information, particularly the spectroscopic factors or amplitudes but occasionally also the spin-parity, that we wish to extract from direct reaction data. It was demonstrated that the DWBA can fail to give a satisfactory description of transfer data and that while the use of more physically sophisticated models can rectify many of the deficiencies of the DWBA it is not a panacea for all ills — recall the problem with the $5/2^+$ state

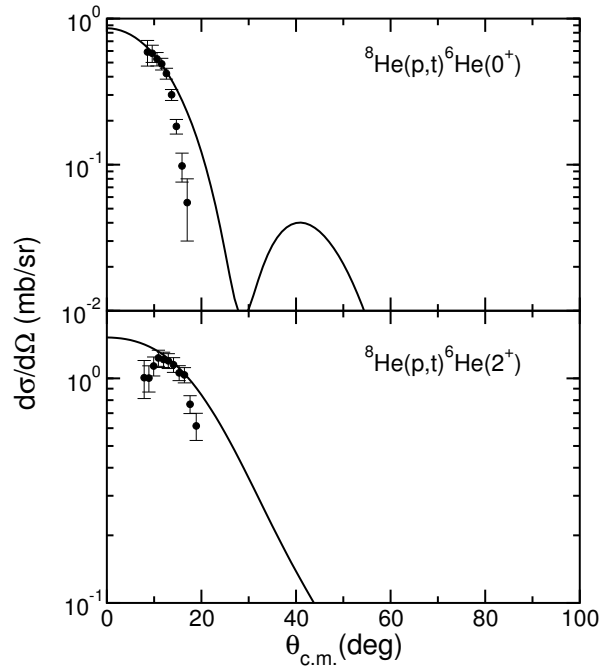


FIGURE 27. Results of the CDCC/CRC calculation for the ${}^8\text{He}(p,t){}^6\text{He}$ reaction at 61.3 A.MeV. The data are taken from [25].

in ${}^{13}\text{C}$. However, when the tenets of the theory are fulfilled DWBA can work very well and will yield the same results as the most sophisticated model e.g. the ${}^{124}\text{Sn}(d,p){}^{125}\text{Sn}$ reaction at low incident deuteron energy. When these conditions are violated, as for instance for the ${}^8\text{He}(p,t){}^6\text{He}$ reaction, the DWBA will fail to provide a coherent picture of data sets at different incident energies and can give misleading results.

There remain a number of important sources of ambiguity in any determination of a spectroscopic factor from direct reaction data quite apart from the choice of reaction model and uncertainties in the data. Perhaps the largest single source of ambiguity derives from the use of the well-depth prescription to calculate the bound-state wave functions. We have seen that different physically reasonable choices of the binding potential well radius can lead to large ($\sim 30\%$) differences in the extracted spectroscopic factors. One could in principle adopt wave functions directly from structure calculations (or adjust the potential well parameters to give equivalent wave functions) to avoid this problem. However, if the structure calculation does not well reproduce the spectrum of the nucleus in question has one really gained much? It has also been suggested that the radius of the potential well should be set equal to the r.m.s. radius obtained from electron scattering on the composite nucleus or that the values of r_0 and a_0 should be constrained such that the binding potential gives the correct r.m.s. matter radius [27] — this is certainly a reasonable possibility for stable nuclei, but at the present time electron scattering measurements are not available for radioactive beams.

The use of global rather than fitted optical potentials can also lead to important differences in the extracted spectroscopic factors. Here we have a “simple” remedy: measure the relevant elastic scattering! However, this is not always practicable (and

of course impossible for exit channels where one of the pair of interacting nuclei is unbound, an increasingly frequent occurrence in radioactive beam studies) but every effort should be made to measure at least the entrance channel elastic scattering. With modern detector arrays such as MUST-2 these measurements may be made at the same time as those for the transfer reaction.

Finally, there are two further effects that influence the extraction of spectroscopic factors from direct reaction data which we have not covered in these lecture notes. These are the Perey effect and “heavy particle stripping”. The Perey effect [28, 29] is a consequence of replacing an intrinsically non-local potential with its local equivalent. The wave functions of the non-local potential are systematically smaller in the nuclear interior than those of the equivalent local potential. This effect can be corrected for in an approximate way and introduces a 10-20 % effect on the extracted spectroscopic factors.

Heavy particle stripping [30] is only relevant for systems with very light targets, e.g. in the ${}^4\text{He}(d,p){}^5\text{He}$ reaction the triton pickup ${}^4\text{He}(d,{}^5\text{He})p$ will also contribute; it is the latter process that is often known as “heavy particle stripping” and its contribution to the final cross section will, in principle, also influence the extracted spectroscopic factors.

ACKNOWLEDGMENTS

The support of the European Commission through the award of a Marie Curie Intra-European Fellowship, contract No. MEIF-CT-2005-010158, is gratefully acknowledged.

REFERENCES

1. P. E. Hodgson, *Nuclear Reactions and Nuclear Structure*, Clarendon Press, Oxford, 1971.
2. G. R. Satchler, *Direct Nuclear Reactions*, Clarendon Press, Oxford, 1983.
3. D. G. Kovar, N. Stein, and C. K. Bockelman, *Nucl. Phys.* **A231**, 266 (1974).
4. S. T. Butler, *Phys. Rev.* **80**, 1095 (1950).
5. L. D. Knutson and W. Haeberli, *Prog. Part. Nucl. Phys.* **3**, 127 (1980).
6. L. L. Lee and J. P. Schiffer, *Phys. Rev.* **136**, B405 (1964).
7. T. J. Yule and W. Haeberli, *Phys. Rev. Lett.* **19**, 756 (1967).
8. R. V. Reid, Jr., *Ann. Phys. (N.Y.)* **50**, 441 (1968).
9. R. C. Johnson and P. J. R. Soper, *Phys. Rev. C* **1**, 976 (1970).
10. J. D. Harvey and R. C. Johnson, *Phys. Rev. C* **3**, 636 (1971).
11. H. Ohnuma, N. Hoshino, O. Mikoshiba, K. Raywood, A. Sakaguchi, G. G. Shute, B. M. Spicer, M. H. Tanaka, M. Tanifuji, T. Terasawa, and M. Yasue, *Nucl. Phys.* **A448**, 205 (1985).
12. G. Perrin, Nguyen Van Sen, J. Arvieux, R. Darves-Blanc, J. L. Durand, A. Fiore, J. C. Gondrand, F. Merchez, and C. Perrin, *Nucl. Phys.* **A282**, 221 (1977).
13. J. M. Lind, G. T. Garvey, and R. E. Tribble, *Nucl. Phys.* **A276**, 25 (1977).
14. P. D. Greaves, V. Hnizdo, J. Lowe, and O. Karban, *Nucl. Phys.* **A179**, 1 (1972).
15. P. D. Kunz, University of Colorado, <http://spot.colorado.edu/kunz/DWBA.html>.
16. I. J. Thompson, *Comput. Phys. Rep.* **7**, 167 (1988).
17. Haixia An and Chonghai Cai, *Phys. Rev. C* **73**, 054605 (2006).
18. B. A. Watson, P. P. Singh, and R. E. Segel, *Phys. Rev.* **182**, 977 (1969).
19. S. Raman, C. H. Malarkey, W. T. Milner, C. W. Nestor, and P. H. Stelson, *At. Data Nucl. Data Tables*, **36** 1 (1987).
20. J. S. Nodvik, C. B. Duke, and M. A. Melkanoff, *Phys. Rev.* **125**, 975 (1962).
21. D. Spaargaren and C. C. Jonker, *Nucl. Phys.* **A161**, 354 (1971).
22. G. H. Rawitscher, *Phys. Rev. C* **9**, 2210 (1974).

23. K. L. Jones, R. L. Kozub, C. Baktash, D. W. Bardayan, J. C. Blackmon, W. N. Catford, J. A. Cizewski, R. P. Fitzgerald, M. S. Johnson, R. J. Livesay, Z. Ma, C. D. Nesaraja, D. Shapira, M. S. Smith, J. S. Thomas, and D. W. Visser, *Phys. Rev. C* **70**, 067602 (2004).
24. N. Keeley, F. Skaza, V. Lapoux, N. Alamanos, F. Auger, D. Beaumel, E. Becheva, Y. Blumenfeld, F. Delaunay, A. Drouart, A. Gillibert, L. Giot, K. W. Kemper, L. Nalpas, A. Pakou, E. C. Pollacco, R. Raabe, P. Roussel-Chomaz, K. Rusek, J.-A. Scarpaci, J.-L. Sida, S. Stepantsov, and R. Wolski, *Phys. Lett.* **B646**, 222 (2007).
25. A. A. Korshennikov, E. Yu. Nikolskii, E. A. Kuzmin, A. Ozawa, K. Morimoto, F. Tokanai, R. Kanungo, I. Tanihata, N. K. Timofeyuk, M. S. Golovkov, A. S. Fomichev, A. M. Rodin, M. L. Chelnokov, G. M. Ter-Akopian, W. Mittig, P. Roussel-Chomaz, H. Savajols, E. Pollacco, A. A. Ogloblin, and M. V. Zhukov, *Phys. Rev. Lett.*, **90**, 082501 (2003).
26. F. Skaza, N. Keeley, V. Lapoux, N. Alamanos, F. Auger, D. Beaumel, E. Becheva, Y. Blumenfeld, F. Delaunay, A. Drouart, A. Gillibert, L. Giot, K. W. Kemper, R. S. Mackintosh, L. Nalpas, A. Pakou, E. C. Pollacco, R. Raabe, P. Roussel-Chomaz, J.-A. Scarpaci, J.-L. Sida, S. Stepantsov, and R. Wolski, *Phys. Lett.* **B619**, 82 (2005).
27. J. F. Sharpely-Schafer, *Phys. Lett.* **26B**, 652 (1968).
28. F. G. Perey, "The Optical Model with Nonlocal Potentials," in *Direct Interactions and Nuclear Reaction Mechanisms*, edited by E. Clementel and C. Villi, Gordon and Breach, Science Publishers, New York, 1963, p. 125.
29. N. Austern, *Phys. Rev.* **137**, B752 (1965).
30. D. Robson, *Nucl. Phys.* **33**, 594 (1962).